Fundamental limits of NO formation in fuel-rich premixed methane-air flames

van Essen, Vincent Martijn

Chapter 6

A LIF study of the effect of pressure on NO formation in premixed methane flames

6.1 Introduction

As seen in Chapters 4 and 5, the major path for NO formation in fuel-rich methane flames is the Fenimore mechanism. As was discussed in Chapter 1, there are still uncertainties surrounding the Fenimore mechanism, inferred from discrepancies between predicted and measured NO concentrations, and particularly from measurements on fuel-rich atmospheric-pressure flames. For example, the comparison of the measured and calculated NO mole fractions in atmospheric-pressure CH_4/Air flames at equivalence ratio 1.3 [1,2] plotted as a function of the measured flame temperature shows that predictions of chemical mechanisms are ~50% too high for most of the flames studied. In contrast to the observations at atmospheric pressure, fuel-rich low-pressure flames generally show good quantitative agreement between predicted and measured post flame front NO concentrations when equivalence ratio is equal or close to 1.3 using GRI Mech 3.0 [3-5](see Chapter 4 for more details). Besides being performed at low pressure, these studies also utilize oxygen/nitrogen mixtures in which the oxygen fraction is higher than that in air (ranging from 27.5% to 40%) to facilitate the stabilization of the flames, as discussed in Chapter 2. One exception to this was a low temperature study [4], which used an oxidizer composition close to air. While the fact that the low-pressure flames were used as targets in the GRI-Mech optimization study [5] probably contributes to the good agreement observed under conditions similar to those used in optimization, the question arises as to which factors might cause the differences in mechanism performance at low and high pressures.

First, considering the large difference in pressure between the low- (<40 Torr) and atmospheric-pressure flames, and taking into account lack of the experimental studies on the pressure dependence of NO formation in the pressure regime between these extremes, it can not be ruled out that the predictive power of the models tuned at low pressure becomes worse at elevated pressures. Similarly, tuning the chemical mechanism with oxidizer having a different O_2/N_2 ratio than that of air, also resulting in higher flame temperatures, cannot guarantee its performance when normal air is used as oxidizer. In this Chapter we examine the effects of pressure on Fenimore NO formation chemistry in the $CH_4/O_2/N_2$ flames for two O_2/N_2 ratios at fixed equivalence ratio (ϕ=1.3) and flame temperature (~2090 K, see below).

Towards this end, we measure the profiles of temperature and mole fractions of CH and NO using laser induced fluorescence (LIF). The experimental results are again compared with the predictions of one-dimensional flame calculations using GRI Mech 3.0 [5].

6.2 Experimental details

As mentioned above, the equivalence ratio is held constant at 1.3 for two O_2/N_2 ratios: 40/60, as used in Chapters 4 and 5, and that of air. The total flow rates of the gases are chosen such that the post flame front temperature is constant for all pressures. The starting point for determining the pressure dependence of the NO mole fraction is the 35 Torr $CH_4/O_2/N_2$ flame at 4 slpm, discussed in Chapter 4, which has a maximum, post-flame-front temperature of ~2090 K. For experiments performed at higher pressures (>35 Torr), the flow rates of $CH_4/O_2/N_2$ flames are adjusted to keep the temperature close to this value [6]. At this temperature, previous measurements performed at both atmospheric CH_4/Air [1] and low-pressure $CH_4/O_2/N_2$ flames (see Chapter 4) indicate that the post-flame-front NO concentration is only a weak function of flame temperature; variations in flame temperature of ± 100 K affects the post-flame NO mole fraction by less than 20%, comparable to our measurement uncertainty. Thus, some degree of flexibility in the ultimate temperature is available without compromising the results. Unfortunately, as discussed in Chapter 2, in our current setup ϕ=1.3 premixed CH_4/Air flames do not exist at pressures below 40 Torr. For this reason, the starting pressure for CH_4/Air flames is 40 Torr. The flow rates of the CH_4/Air flames are close to free flame velocities for every pressure (>40 Torr) to approach the target temperature of ~2090 K. The exit velocity of the cold gases for the 40 Torr CH_4/Air flame matched the free flame burning velocity. All flames are visually flat with the exception of the 40 Torr CH_4/Air flame, which is slightly curved at the edges of the flame.

For experiments at pressures between 35 and 500 Torr, the burner is located inside the vacuum chamber as described in Chapter 2. Because water condensation on the quartz view ports prevented performing measurements of species and temperature for pressures above 500 Torr, atmospheric pressure measurements are performed on flames burning in the open air.

The profiles of flame temperature and mole fractions of OH, CH and NO are determined using linear LIF as described in Chapter 3. The CH mole fractions are determined in a limited number of low-pressure flames; with increasing pressure the profiles become too narrow to measure in the current setup. The quenching rates for pressures up to ~100 Torr are determined from the temporal LIF-signal using the method described in Chapter 3. Since at higher pressures (>100 Torr) the time resolution of our detection system is comparable to or larger than the fluorescence lifetimes, quenching rates for pressures >100 Torr are calculated based on species derived from the CHEMKIN calculations and using cross sections published by Tamura et al. [7]. The comparison of the experimentally determined quenching rates with calculations show good agreement (Chapter 3): for OH within a few percent and for both NO and CH better than ~10%.

The LIF signals for pressures up to 500 Torr are calibrated following the procedure described in Chapter 3. The calibration of the NO-LIF signal for low-pressure flames is performed by seeding the reference flame as discussed in Chapter 3, whereas at atmospheric pressure, calibration is performed by seeding the cold unburned mixture of a ϕ=1.0 premixed CH_4/Air flame (50 slpm). This atmospheric pressure CH_4/Air flame was also used as the calibration flame in previous studies of NO formation from this laboratory [8]. The amount of NO seeded in the cold gas mixture of this flame is 200 ppm. The estimated accuracy of our measurements is better than 15%, 20 % and 20% for CH, NO and OH mole fractions, respectively (see Chapter 3 for details). In addition, the flames are modeled using GRI Mech 3.0 and PREMIX [9], as discussed in the earlier Chapters of this thesis.

6.3 Results and discussion

6.3.1 Temperature and species concentration measurements

To provide an additional consistency check of the experiments, in some flames the OH profiles are measured. The agreement between the experimental and calculated OH data is better than 20% for all flames where OH mole fraction is measured. Typical examples are shown in Figure 6.1 for the measured and calculated OH mole fractions in CH_4/Air flames for 75 and 400 Torr.

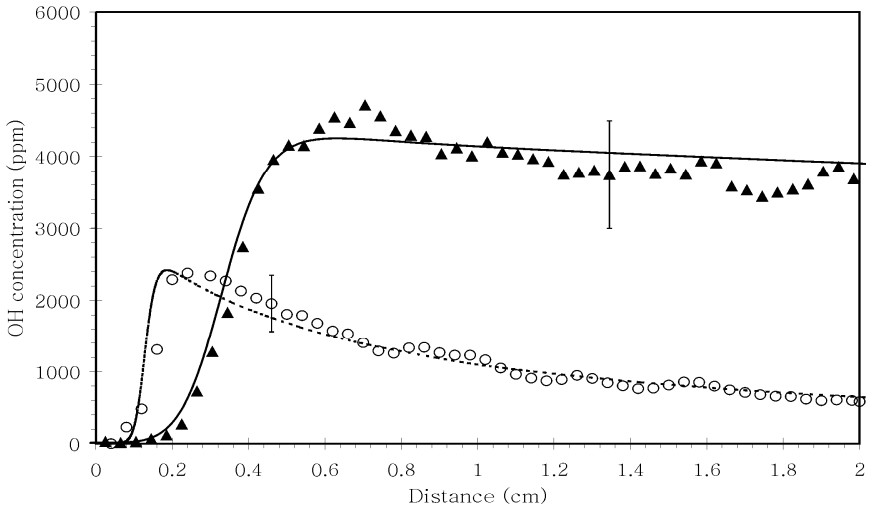

Figure 6. 1 Measured and calculated OH mole fractions for 75 and 400 Torr ϕ=1.3 premixed CH_4/Air flames. Filled triangles denote 75 Torr, open circles 400 Torr. Lines denote calculations: solid, 75 Torr and dashed, 400 Torr.

The excellent agreement between measured and calculated OH mole fractions at 75 and 400 Torr maintains our confidence in the adequacy of both the temperature measurements and the one-dimensional assumption for modeling the flames.

Examples of the profiles of temperature and mole fractions of NO and CH in methane/air flames are given in Figure 6.2, at pressures of 40, 75 and 400 Torr, respectively. The temperature profiles for all flames studied are flat within the uncertainties of measurements after the initial rise; the steepness of this rise clearly increases with the pressure. The experimental NO profiles show rapid growth in the flame front, and in the post-flame region are then either flat (at pressures above ~ 200 Torr) or show a modest growth (<200 Torr), which does not exceed ~ 5 ppm for all flames studied. The position of the experimental CH profiles, measured in the low-pressure CH_4/Air (Figures 6.2A and 6.2B) and the $CH_4/O_2/N_2$ flames (Chapter 4), coincides with the location of the rapid rise in the NO profiles, indicating the Fenimore origin of the NO in these flames.

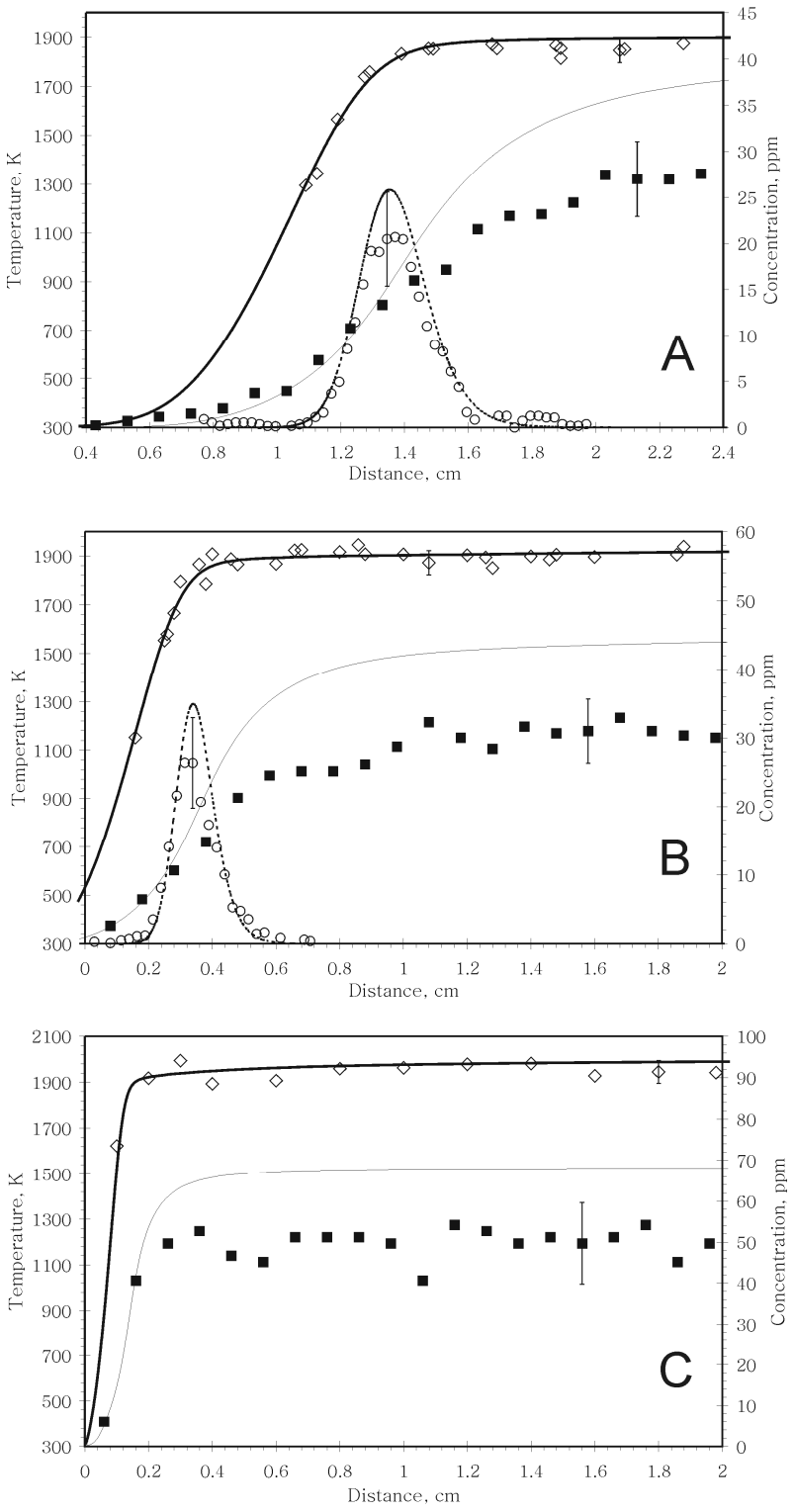

Figure 6. 2. Measured and calculated profiles of temperature and CH and NO mole fraction for ϕ=1.3 premixed CH_4/Air flames at 40 Torr (A), 75 Torr (B) and 400 Torr (C). Filled squares denote NO, circles denote CH mole fractions multiplied by 2(Figure A) or 3(Figure B). Diamonds denote temperatures. Lines denote calculations: thick solid lines: temperature, thin solid lines: NO, dashed lines: CH

Figure 6.2 also includes the calculated temperature and species profiles using CHEMKIN calculations obtained by solving the energy equation. The comparatively broad reaction zone in the low-pressure flames allowed us to resolve the initial temperature rise at these pressures with reasonable detail, see Figures 6.2A-B and Chapters 4-5. The temperature and CH and NO profiles calculated using the fit to the measured temperatures (Chapter 3) are practically indistinguishable from those calculated solving the energy equation (the discrepancies are substantially smaller than the experimental uncertainties)**.** For this reason, we compare the experimental data with the CHEMKIN results obtained by solving the energy equation in the discussion below.

The calculated NO profiles using GRI Mech 3.0 show good agreement with measured profiles for $CH_4/O_2/N_2$ flames (as seen in Chapter 4), but overpredict NO profiles for CH_4/Air flames (see Figure 6.2). The rate-of production-analysis indicates that the rise in the NO profile in the flame front is predominantly caused by the Fenimore mechanism, while the calculations also show that the slow growth in the post flame zone of the low-pressure flames is mainly from the Zeldovich mechanism. The comparison of the measured and calculated CH profiles reveals an excellent agreement in terms of both the peak CH location and width of the CH profiles for CH_4/Air (Figures 6.2A-B) and $CH_4/O_2/N_2$ flames (Chapter 4). The agreement between experimental and calculated peak CH mole fractions is quantitative for $CH_4/O_2/N_2$ flames and just outside the error bars for CH_4/Air flames, where peak CH mole fractions are slightly overpredicted.

6.3.2 Pressure dependence of NO formation

To facilitate the further discussion on the variation in the NO mole fraction with pressure, we plot measured NO mole fractions and maximum temperature as a function of the pressure. To reflect NO formed via Fenimore mechanism, we used the NO mole fraction in the post flame front region where most of the NO profiles are flat or show only a slow increase, generally at 1.6 cm above the burner surface, with the exception of 40 Torr CH_4/Air flame where the NO mole fraction is taken at 2.2 cm (see Figure 6.2A). We emphasize that the choice of the point is irrelevant for all pressures higher than 120 Torr (the NO profiles are flat), and only of the minor importance for

flames at lower pressure. The post-flame-front increase in the NO mole fraction is always within the accuracy of the NO measurements. These plots are shown in Figures 6.3A and 6.3B for $CH_4/O_2/N_2$ and CH_4/Air flames, respectively.

Since previous studies (see Refs. [1,2,10] and Chapters 4) have shown that burner stabilization is an important factor in NO formation, it is instructive to consider changes in the degree of stabilization as function of pressure. In the $CH_4/O_2/N_2$ flames, the adiabatic temperature (T_{add}) increases from 2469K to 2678 K when going from 35 to 761 Torr; that the measured temperature remains constant at ~2090 K indicates heat loss to the burner that is both substantial and increasing with pressure. Since CH_4/Air flames are close to free flame velocity, heat transfer to the burner is of less importance when changing pressure.

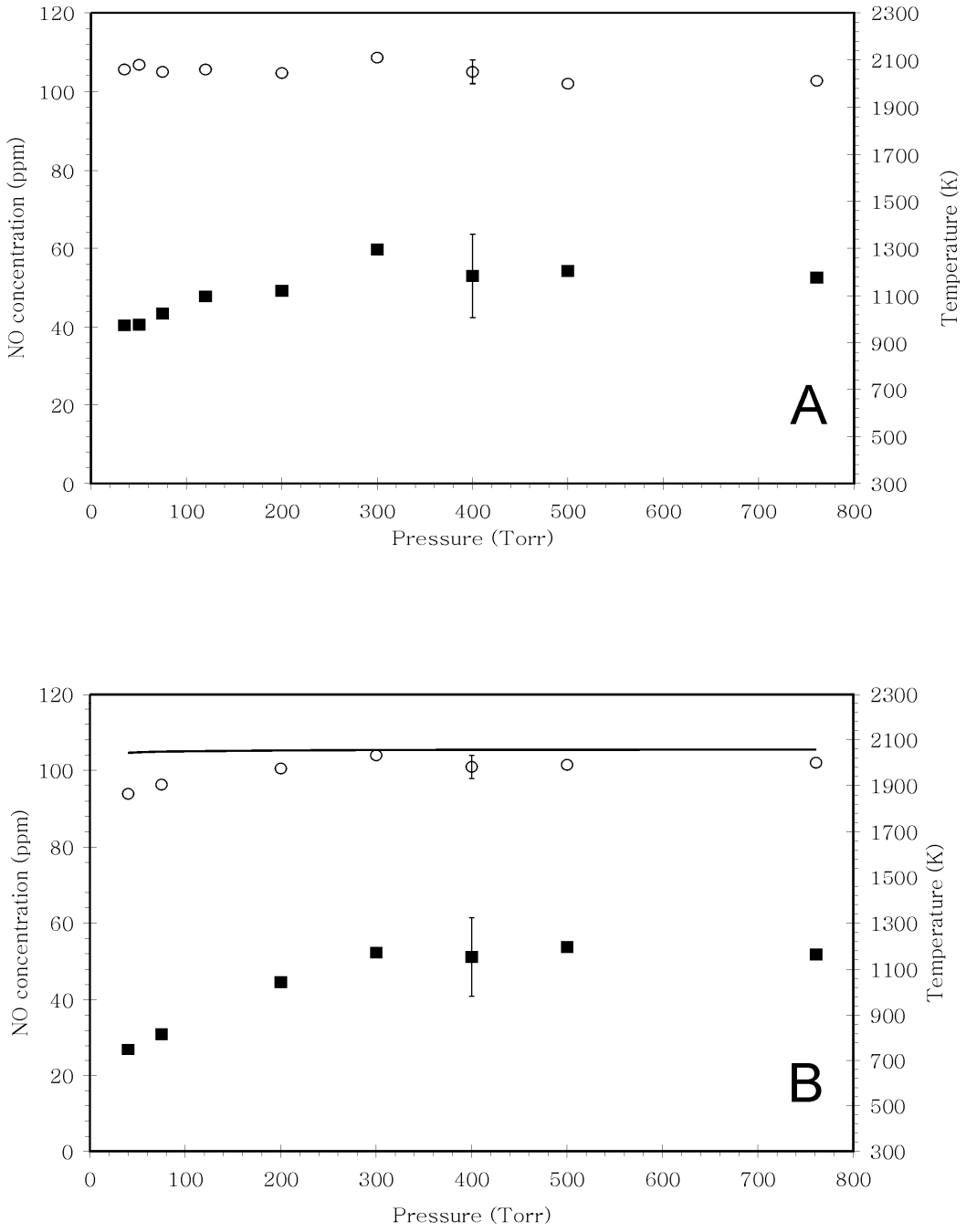

Figure 6. 3. Measured temperature and NO mol fractions for $CH_4/O_2/N_2$ flame (A) and CH_4/Air flame (B). The line Figure B denotes calculated adiabatic flame temperature. Open circles denote temperature, closed squares denote NO.

Figure 6.3 shows that the measured NO mole fraction is a weak function of pressure for both $CH_4/O_2/N_2$ and CH_4/Air flames, at constant flame temperature. A small increase in measured NO mole fraction going from the lowest pressure to ~200 Torr is observed. This increase is within the

uncertainty of measurements for the $CH_4/O_2/N_2$ flames. However, for CH_4/air flames the small increase in measured NO mole fraction is just outside the uncertainty, which could be a result of a small increase in measured temperature. Further pressure increase does not affect the NO mole fraction, regardless of substantial differences in the mass flux and pressure for both types of flame. It is also interesting to note that at pressures above ~200 Torr, despite the differences in O_2/N_2 ratios and degrees of stabilization, all flames produce the same amount of NO. This observation is being studied further.

6.3.3 Comparison with model predictions

Figure 6.4 presents the ratio of the NO mole fraction calculated by GRI Mech 3.0 to that measured as a function of pressure for CH_4/Air and $CH_4/O_2/N_2$ flames.

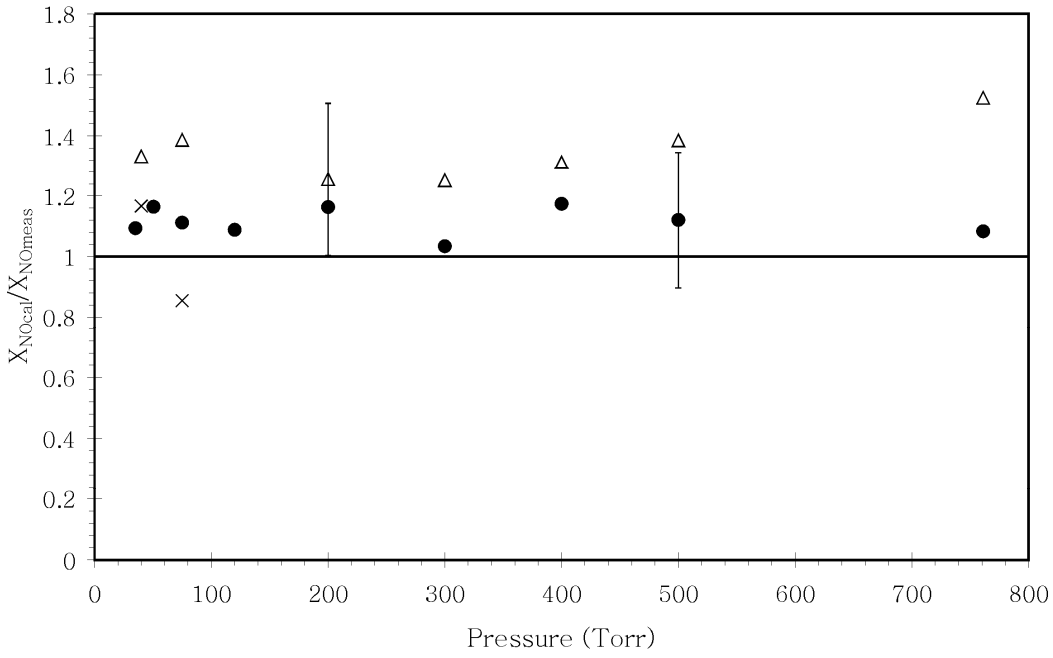

Figure 6. 4 Ratio of calculated and measured NO mole fractions. Filled circles denote $CH_4/O_2/N_2$ flame and open triangles, CH_4/Air flame. Crosses denote the calculated amount of Fenimore NO (see text for details).

The calculated NO mole fractions are taken at the same distance from the burner surface as the measured data. As can be seen from Figure 6.4, the $CH_4/O_2/N_2$ flames show very good agreement between the measured and

calculated NO mole fractions, being always 20% or better. The predictions of the NO mole fraction are 30% or higher above the measured values for the pressure domain studied; this over prediction increases to nearly 50% at atmospheric pressure, in agreement with previous studies [1,2,10].

Keeping in mind the good predictive ability of GRI Mech 3.0 for NO and CH mole fraction and temperature in the $CH_4/O_2/N_2$ flames, and with an eye towards the quantitative disagreement between the measured and calculated NO mole fraction in CH_4/Air flames, it is of interest to estimate the expected amount of Fenimore NO ($X_{NO,Fen}$) using equation (1.11) in the low-pressure CH_4/Air flames at 40 and 75 Torr using both experimental and calculated CH and temperature profiles. The ratio of calculated $X_{NO,Fen}$ to measured NO mole fraction is shown in Figure 6.4.

The agreement between the measured NO mole fractions and $X_{NO,Fen}$ is very good (within 15%), similar to that observed at 25 and 35 Torr. As discussed in Chapter 4, this demonstrates the degree of internal consistency between the experimental CH and NO mole fraction profiles and the adequacy of the rate coefficient for $CH+N_2$, giving us confidence in the reliability of the results. Returning to Figure 6.2, we recall that the peak CH mole fraction was overpredicted by GRI-Mech, outside the limits of uncertainty. Since nearly all NO formed in these flames comes from the Fenimore mechanism, which was quantitatively predicted for the $CH_4/O_2/N_2$ flames, we conclude that the overprediction of the NO mole fraction in the 40 and 70 Torr CH_4/air flames is caused by the observed overprediction of the CH profile. Given the structural overprediction of the NO mole fraction for the CH_4/air flames in Fig. 6.4, we suggest that the overprediction of the CH mole fraction is responsible for this at higher pressures as well. Although very difficult, measurements of the CH profiles at higher pressures are recommended to confirm this suspicion.

6.4 Conclusions

We investigated the effects of pressure on NO formation in methane flames with two different O_2/N_2 ratios (40/60 and that of air), at constant equivalence ratio (ϕ=1.3) and constant flame temperature ~2090 K. Changing the pressure in the range 35 - 761 Torr, we observe from the CHEMKIN calculations that NO formation occurs predominantly from the Fenimore mechanism independent of pressure and O_2/N_2 ratio in the oxidizer. When

plotted as a function of pressure, the NO mole fraction at constant flame temperature for different O_2/N_2 ratios is seen to be a very weak function of pressure. We also observed that the post-flame NO mole fraction is independent of the O_2/N_2 ratio in the most of the pressure domain studied. Detailed calculations using GRI-Mech 3.0 predicted the trend of the measured NO pressure dependence qualitatively for both O_2/N_2 ratios. The predictions show a quantitative agreement for the $CH_4/O_2/N_2$ flames, but overpredict the NO mole fraction by more than 30% for the CH_4/air flames. We suggest that the observed differences in the CH_4/air flames may be addressed by improving the predictions of the CH mole fraction.

Bibliography

1. Sepman, A. V, Mokhov, A. V., and Levinsky, H. B., "A Laser-Induced Fluorescence and Coherent Anti-Stokes Raman Scattering Study of NO Formation in Preheated, Laminar, Rich Premixed, Methane/Air Flames", *Symp.(Int.) Combust.* **29**, 2187-2194 (2002)

2. Mokhov, A. V. and Levinsky, H. B., "*A LIF and CARS Study of the Effects of Upstream Heat Loss on NO Formation From Laminar Premixed Burner-Stabilized Natural-Gas/Air Flames*", 26th Symp. (Int.) Combust., 2147-2154 (1996)

3. Berg, P. A., Hill, D. A., Noble, A. R., Smith, G. P., Jeffries, J. B., and Crosley, D. R., "Absolute CH Concentration Measurements in Low-Pressure Methane Flames: Comparisons With Model Results", *Combust.Flame* **121**, 223-235 (2000)

4. Pillier, L., El Bakali, A., Mercier, X., Rida, A., Pauwels, J. F., and Desgroux, P., "*Influence of C-2 and C-3 Compounds of Natural Gas on NO Formation: an Experimental Study Based on LIF/CRDS Coupling*", 30th Symp. (Int.) Combust., 1183-1191 (2005)

5. Smith, G. P., Golden, D. M., Frenklach, M., Moriarty, N. W., Eiteneer, B., Goldenberg, W., Bowman, C. T., Hanson, R., Gardiner, W. C, Lissianski, V., and Qin, Z., http://www.me.berkeley.edu/gri_mech/.

6. Sepman, A. V., *Effects of the burner stabilization on nitric oxide formation and destruction in atmospheric-pressure flames*, Rijksuniversiteit Groningen, 2006

7. Tamura, M., Berg, P. A., Harrington, J. E., Luque, J., Jeffries, J. B., Smith, G. P., and Crosley, D. R., "Collisional Quenching of CH(A), OH(A), and NO(A) in Low Pressure Hydrocarbon Flames", *Combust.Flame* **114**, 502-514 (1998)

8. Mokhov, A. V., Levinsky, H. B., and van der Meij, C. E., "Temperature Dependence of Laser-Induced Fluorescence of Nitric Oxide in Laminar Premixed Atmospheric-Pressure Flames", *Appl.Opt.* **36**, 3233-3243 (1997)

9. Kee, R. J., Rupley, F. M., and Miller, J. A., "CHEMKIN II: A Fortran Chemical Kinetics Package for the Analysis of Gas-Phase Chemical Kinetics", Report No.SAND89-8009, Sandia National Laboratories ,1989

10. Mokhov, A. V. and Levinsky, H. B., "*A LIF and CARS Investigation of Upstream Heat Loss and Flue-Gas Recirculation As NOx Control Strategies for Laminar, Premixed Natural-Gas/Air Flames*", 28th Symp. (Int.) Combust., 2467-2474 (2000)